

# Special Report 87-14

July 1987

(4) (S)

DTIC FILE COPY



## *Saline ice penetration* *A joint CRREL-NSWC test program*

David M. Cole and Howard K. Steves

AD-A189 206

DTIC  
ELECTE  
DEC 07 1987  
S D  
CE

*Area 189 206*

**REPORT DOCUMENTATION PAGE**

Form Approved  
OMB No 0704-0188  
Exp. Date Jun 30, 1986

1a. REPORT SECURITY CLASSIFICATION Unclassified		1b. RESTRICTIVE MARKINGS	
2a. SECURITY CLASSIFICATION AUTHORITY		3. DISTRIBUTION/AVAILABILITY OF REPORT Approved for public release; distribution is unlimited.	
2b. DECLASSIFICATION/DOWNGRADING SCHEDULE		4. PERFORMING ORGANIZATION REPORT NUMBER(S) Special Report 87-14	
5. MONITORING ORGANIZATION REPORT NUMBER(S)		6a. NAME OF PERFORMING ORGANIZATION U.S. Army Cold Regions Research and Engineering Laboratory	
6b. OFFICE SYMBOL (if applicable) CECRL		7a. NAME OF MONITORING ORGANIZATION	
6c. ADDRESS (City, State, and ZIP Code) Hanover, New Hampshire 03755-1290		7b. ADDRESS (City, State, and ZIP Code)	
8a. NAME OF FUNDING/SPONSORING ORGANIZATION		8b. OFFICE SYMBOL (if applicable)	
9. PROCUREMENT INSTRUMENT IDENTIFICATION NUMBER		8c. ADDRESS (City, State, and ZIP Code)	
10. SOURCE OF FUNDING NUMBERS		9. PROCUREMENT INSTRUMENT IDENTIFICATION NUMBER	
PROGRAM ELEMENT NO.	PROJECT NO. 4A1611 01A91D	TASK NO. 00	WORK UNIT ACCESSION NO. 424
11. TITLE (Include Security Classification) SALINE ICE PENETRATION A Joint CRREL-NSWC Test Program			
12. PERSONAL AUTHOR(S) Cole, David M. and Steves, Howard K.			
13a. TYPE OF REPORT	13b. TIME COVERED FROM _____ TO _____	14. DATE OF REPORT (Year, Month, Day) July 1987	15. PAGE COUNT 41
16. SUPPLEMENTARY NOTATION			
17. COSATI CODES		18. SUBJECT TERMS (Continue on reverse if necessary and identify by block number)	
FIELD	GROUP	SUB-GROUP	Ice Ice penetration tests Ice perforation tests
			Projectiles Sea ice
19. ABSTRACT (Continue on reverse if necessary and identify by block number) This paper reports on the response of a floating saline ice sheet to penetration and perforation by 25.4-mm-diameter projectiles with three nose shapes: a full cone, a truncated cone and a full flat. Impact velocity was varied to produce behavior ranging from slight penetration to complete perforation of the 210- to 280-mm-thick ice sheet. The extent of crushing and fracturing adjacent to the path of the projectile was quantified, indicating the existence of a zone of crushing extending 1 to 2 body diameters into the ice sheet from the cavity wall. A series of shots into free-floating targets indicated that for penetrations of roughly two-thirds of the sheet thickness, the depth of penetration did not vary significantly as the target size was reduced to 24 body diameters. Tests on coated projectiles indicated that no significant abrasion occurred between the ice and the nose area of the projectile. Information is also presented on the effects of gun pressure, nose shape, average sheet temperature and angle of attack on the depth of penetration.			
20. DISTRIBUTION/AVAILABILITY OF ABSTRACT <input checked="" type="checkbox"/> UNCLASSIFIED/UNLIMITED <input type="checkbox"/> SAME AS RPT <input type="checkbox"/> DTIC USERS		21. ABSTRACT SECURITY CLASSIFICATION Unclassified	
22a. NAME OF RESPONSIBLE INDIVIDUAL David M. Cole		22b. TELEPHONE (Include Area Code) 603-646-4100	22c. OFFICE SYMBOL CECRL-EA

PREFACE

This report was prepared by David M. Cole, Research Civil Engineer, Applied Research Branch, Experimental Engineering Division, U.S. Army Cold Regions Research and Engineering Laboratory, and Howard K. Steves, Hydroballistics Test Facility Manager, Naval Surface Weapons Center. It was jointly funded by CRREL through DA Project 4A161101A91D, In-House Laboratory Independent Research; Task 00; Work Unit 424, Saline Ice Penetration; and the Naval Surface Weapons Center, White Oak, Maryland. The authors are grateful for the valuable assistance of C. Purves, L. Resch and E. Bishop from NSWC and to R. Roberts, N. Perron and J. Richter-Menge from CRREL.

This report has been technically reviewed by Dr. M. Kleinerman of NSWC and Dr. M. Mellor of CRREL.

The contents of this report are not to be used for advertising or promotional purposes. Citation of brand names does not constitute an official endorsement or approval of the use of such commercial products.

Accession For	
NTIS GRA&I	<input checked="" type="checkbox"/>
DTIC TAB	<input type="checkbox"/>
Unannounced	<input type="checkbox"/>
Justification	
By _____	
Distribution/ _____	
Availability Codes	
Dist	Avail and/or Special
A-1	



## CONTENTS

	<u>Page</u>
Abstract .....	1
Preface .....	11
Introduction .....	1
Materials and methods .....	3
Test site .....	3
Test equipment and instrumentation .....	3
Model characteristics .....	5
Testing procedure .....	7
Characterization of ice after testing .....	8
Results and discussion .....	9
General .....	9
Abrasion during ice entry .....	11
Macroscopic observations .....	12
Thin section observations .....	17
Additional observations .....	28
Additional discussion and recommendations .....	31
Conclusions .....	33

## ILLUSTRATIONS

### Figure

1. Thin sections of the naturally grown ice sheet .....	2
2. Salinity profile for the ice sheet .....	3
3. A block of test material .....	4
4. Test site .....	4
5. Projectiles used in this study .....	6
6. Test point locations on ice sheet .....	7
7. Location of vertical and horizontal thin sections .....	9
8. Projectile after shot 18 .....	11
9. Typical test points after firing .....	13
10. Block of ice containing two test points .....	14
11. Test point after firing a reference shot at low temperature ..	14
12. Crater of shot fired at 60° to the horizontal .....	15
13. Example of a low velocity shot where the projectile did not lodge firmly in the ice, but remained in the cavity .....	16
14. Example of a very low velocity shot that failed to lodge in the ice .....	16
15. Penetration vs gun pressure for the three nose shapes .....	18
16. Vertical thin section photographs of the point areas for the three nose shapes .....	19
17. Vertical thin section adjacent to the path of the projectile in shot 27 .....	20
18. Typical horizontal thin section from the upper part of the ice sheet .....	21
19. Back-lit thick section of the tip of the cavity from shot 28 .	22
20. Vertical thin section along the cavity from shot 17 .....	23

Figure		Page
21.	Vertical thin section along cavities resulting from perforation.	24
22.	Unusual crater formed by shot 18 .....	25
23.	Vertical thin sections along the path of penetration of shot 18.	26
24.	Shot 28, fired at an angle of 60° to the horizontal .....	28
25.	Vertical thin section of laboratory-grown saline ice .....	30
26.	Shot 42, fired into laboratory-grown saline ice .....	31

**TABLES**

Table		
1.	Model characteristics .....	6
2.	Summary of saline ice penetration test results .....	10

## SALINE ICE PENETRATION

A Joint CRREL-NSWC Test Program

by

David M. Cole and Howard K. Steves

### INTRODUCTION

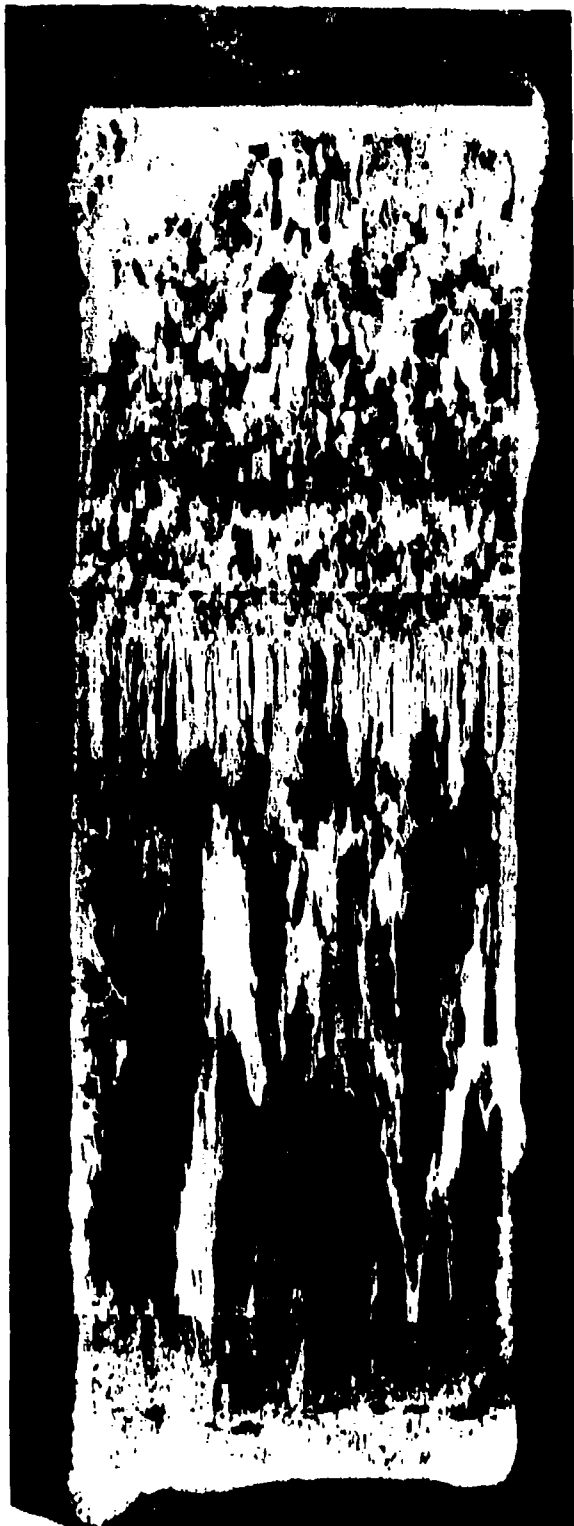
The response of saline ice to impact by kinetic energy penetrators is currently of great interest to the defense community. Efforts to model the penetration or perforation event\* require a knowledge of the ice properties and an understanding of how the ice deforms during various stages of the event. This report describes a test program designed to further our understanding of the mechanics of the penetration event through careful examination of the ice after penetration.

A series of ice penetration tests was carried out under a joint project involving personnel from CRREL and the Naval Surface Weapons Center (NSWC). The objective of these tests was to investigate the response of a saline ice sheet, nucleated and grown outdoors in the winter of 1984-85, to penetration and perforation by projectiles. By "response" we mean detectable changes in the ice structure, including depth of penetration, crater size and shape, extent of macro- and micro-fracturing and the extent and location of zones of local crushing or recrystallization. We tested various projectile nose shapes and masses as well as impact velocities and angles.

This investigation leads to a better understanding of the deformational processes in the ice during the penetration-perforation event and thus will provide insight useful in modeling efforts.

---

\* In this report, penetration means that the projectile entered the ice sheet but did not pass through; perforation means that the projectile passed completely through the ice.



a. Vertical.



b. Horizontal.

Figure 1. Thin sections of the naturally grown ice sheet.

## MATERIALS AND METHODS

### Test site

All tests were run at CRREL in January 1985. A naturally grown saline ice sheet was used for all but one of the tests. At the start of testing, the sheet was approximately 210 mm (8.5 in.) thick. Because of several extremely cold nights, the sheet grew to approximately 280 mm (11 in.) thick by the end of the testing period. Figure 1 shows vertical and horizontal thin sections\* of the sheet and Figure 2 gives the salinity profile. Note the relatively fine-grained discontinuous columnar material to a depth of approximately 100 mm (4 in.). Figure 3 shows a photograph of a block of the test material that had been removed from the sheet.

The sheet was grown in a 10- by 10- by 1-m concrete pool. The salinity was 24 ‰ prior to freezing. The average salinity of the ice was 4.3 ‰ and the bulk density was 0.866 Mg/m<sup>3</sup>.

### Test equipment and instrumentation

#### General

The test program used an air gun, with associated triggering and timing mechanisms, to launch the projectiles and two high-speed cameras with flash units and timing devices to record both the projectile motion during entry and the ejecta patterns.

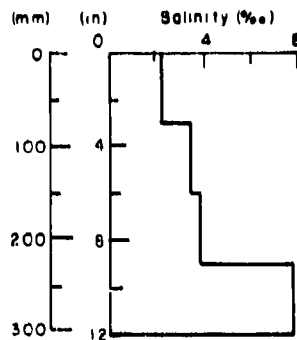


Figure 2. Salinity profile for the ice sheet.

\* The photographs of the vertical thin sections are generally formed from several smaller photographs. Slight differences in the shading of each individual photograph can cause a banded appearance in the composite. This should not be confused with the banded structure resulting from changes in crystal size and shape.



Figure 3. A block of test material. Note discontinuity in structure corresponding to the onset of purely columnar growth.

Figure 4 shows the test site. The air gun, which could be fired at angles between  $60^\circ$  and  $90^\circ$  to the ice surface, was mounted on a rolling crosswalk that spanned the test pool. The crosswalk was easily moved manually along the length of the pool, allowing us to quickly reposition the air gun over each test point. The two high-speed cameras were mounted



Figure 4. Test site.

on the crosswalk as well. The following sections describe the air gun and carrier systems in greater detail.

### Air Gun

All tests were conducted using an air gun with a quick opening valve design to allow pressures up to 5.17 MPa (750 lb/in.<sup>2</sup>) to drive the projectiles. The barrel diameter could be varied on this particular gun, although in these tests a 25.4-mm (1-in.) diameter barrel was used. The driving gas was dry nitrogen, which was both convenient to use and readily available. Before bringing the gun to CRREL, NSWC made a number of test shots to check its performance. Two reluctance pickups were used at the end of the barrel to measure the exit velocity of the projectile. Preliminary test runs with this equipment at room temperature indicated satisfactory operation. However, the timing system worked sporadically in the cold and consequently velocity measurements were not obtained for every shot.

### Photography

Two Hycam high-speed cameras, running at 4000 frames per second, provided photographic records of the penetration events. One camera was positioned directly to the side of the gun, looking down on the test point, and the other was positioned at the far end of the crosswalk, viewing the impact from the side.

Two flashbulb reflectors with No. 31 flashbulbs were used: one positioned near the side camera and the other on the ice, close to the top camera. The available light from these bulbs lasts only 100 ms, so a delay triggering system was used that coordinated camera start, gun firing and flash trigger. Additionally, we used two counters to measure the time between the triggering of the two reluctance pickups for velocity calculations.

### Model characteristics

We tested the three nose shapes shown in Figure 5. All projectile models were 25.4 mm (1 in.) in diameter with lengths and weights given in Table 1. The straight cone approximates a shape used by Sandia National Laboratories, Livermore, in previous ice penetration tests. The 0.5 D flat (i.e., the diameter of the flat region is one-half the body diameter) on a conical section was chosen because it is a stable water-entry shape with a

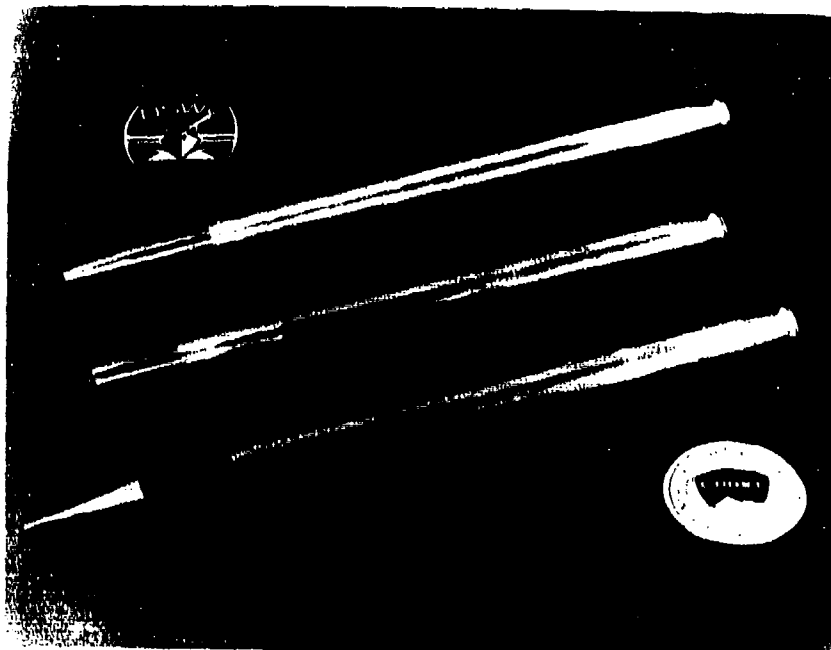


Figure 5. Projectiles used in this study.

Table 1. Model characteristics.

Nose	Weight (g [lb])	Length (mm [in.])
Full cone	545 [1.20]	451 [17.75]
0.5 D flat cone	554 [1.22]	419 [16.5]
Full flat	459 [1.01]	387 [15.25]

relatively low drag. The full flat that was tested is also stable during water entry but has a high drag coefficient and was used only for comparison.

The conical noses had a small section of aluminum at the tip to prevent damage to the bottom of the test pool when the model perforated the ice. The afterbody of these models consisted of aluminum tubing with a tail plug designed to take advantage of cavity stabilization during water entry. When the body tries to turn during water entry this tail comes into contact with the cavity wall and provides a restoring force to the model. All models used the same tail configuration, although the 0.5 D and full

flat noses would not normally need the cavity stabilizing tail. The projectiles were designed with future water-entry tests in mind. Before the models were fired into the ice at CRREL, a few tests were made at NSWC to check their stability during water entry. The length of the models was fixed at this time because a shorter cone model was found to be unstable during oblique water entry.

Testing procedure

The crosswalk was moved an appropriate distance (at least 0.3 m [1 ft]) between shots and the gun was relocated on the bridge three times as the testing progressed. Test points generally occur in sequence from south to north on each line of fire (Fig. 6). Prior to freezeup, we placed armor plating under the first line of fire, approximately 1 m from the east edge of the pool, and extending 4.9 m (~ 16 ft) from the south edge of the pool. All perforation shots were fired in this region.

As testing proceeded, we periodically removed blocks of ice containing the test point to examine the fracturing and microstructural changes in the laboratory. The ice was cut with an electric chain saw and the resulting

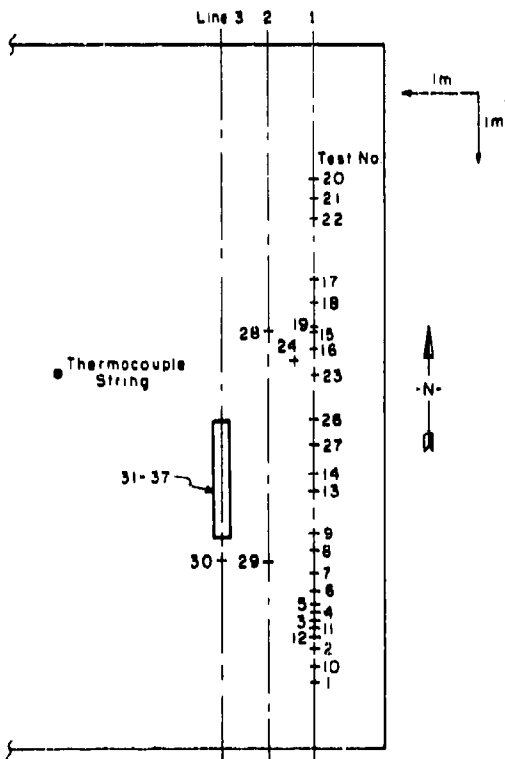


Figure 6. Test point locations on ice sheet.

blocks were subsequently wrapped in polyethylene and stored in a coldroom until sectioning.

A thermocouple string located at the center of the sheet provided temperature readings at 25-mm (1-in.) intervals through the ice. Readings were taken periodically throughout the day. Air temperature readings were also taken during the test period.

Most shots were fired into the nominally intact ice sheet. The sheet was floating on approximately 0.7 m of water and was solidly frozen to the sides of the concrete pool. Additionally, to investigate the effect of target size on the penetration event, square specimens of varying sizes were cut free from the ice sheet and floated under the air gun for testing, after which the blocks were removed from the water and photographed.

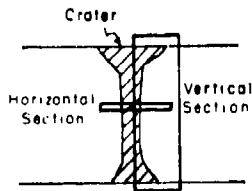
In general, test shots were fired at 90° to the horizontal. However, several were fired at 60° to study the change in fracture pattern and penetration distance. In all tests, measurements of the depth of penetration were taken along with measurements of the final angle of the projectile, when applicable.

Since little is known about the effects of ice structure on the penetration event, we tested a large specimen of laboratory-grown saline ice having significantly different structural characteristics than the naturally grown ice sheet. The laboratory-grown saline ice was the same type of material used in an ice penetration study by Sandia National Laboratories, Livermore, and is very similar to first-year sea ice. To achieve the appropriate thermal regime, the 0.76-m-diameter, 0.38 m-high (30-in.-diameter, 15-in.-high) block of laboratory-grown ice was placed in the pool overnight and used for a reference test the following morning.

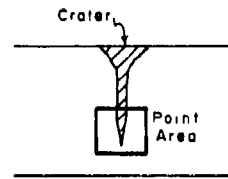
#### Characterization of ice after testing

Immediately after firing, the impact point was photographed and the crater was cleared of loose debris and measured. An approximately 0.3-m<sup>2</sup> (1-ft<sup>2</sup>) area centered on the impact point was then cut from the sheet as detailed earlier. In all, we selected 17 of the total of 44 test shots for thin section analysis.

These blocks were stored in a coldroom at -12°C (10°F) for up to several weeks until thin sectioning. Figure 7 shows the location of the vertical and horizontal thin sections relative to the point of impact of



a. Perforation shot.



b. Penetration shot.

Figure 7. Location of vertical and horizontal thin sections in a tested block.

the projectile for both perforating and penetrating shots. These thin sections allow us to determine the zones of crushing and fracturing about the cavity. These data are expected to yield useful information regarding the distribution of stresses in the ice during the penetration event.

## RESULTS AND DISCUSSION

### General

Table 2 gives information on each test, including test number, nose shape, gun pressure, projectile velocity, length of penetration, average temperature over the path of penetration, the angle between the projectile and horizontal (if other than  $90^\circ$ ), and crater dimensions.

As with any test program conducted out of the laboratory, some variables were out of our control. The most notable of these are ice thickness, ice structure and temperature. As noted above, over the course of testing the ice grew in thickness from 216 mm (8-1/2 in.) to 279 mm (11 in.). The natural nucleation and freezing conditions result in the two-layered structure seen in Figure 1. Additionally, the ambient temperature varied widely during testing, ranging from  $-22^\circ\text{C}$  ( $-6^\circ\text{F}$ ) to near freezing. As a consequence, the temperature of the upper portions of the ice sheet varied as well. Fortunately, as will be discussed in detail below, the results indicate that neither structure nor the variations in temperature gradient had a significant effect on the depth of penetration of the projectiles. Some differences were noted, however, in how the ice deformed. The extent of the cracking associated with crater formation about the point of impact was the most obvious difference between the tests run at low and high surface temperatures. At the lower temperatures, a network of cracks

Table 2. Summary of saline ice penetration test results.

Shot no.	Model id.	Gun pressure (MPa)	Crater** Perf** dia.	Crater** depth	Avg† temp (°C)	Ice† thick (m)	Model wt (g)	Velocity (m/s)	Air temp (°C)	Day/ time	Comments	
1	a	3.45	(perf)	5.0	1.5	-	0.216	540	-4.2	1/pm	Model hit bottom of pool.	
2	b	3.45	(perf)	5.0	2.0	-	0.216	553	-	1/pm		
3	a	0.69	1.75	5.0	1.75	-	0.216	554	-4.2	1/pm		
4	a	1.38	2.25	0.0	0.0	-	0.216	554	-4.2	1/pm	Bounce out.	
5	a	2.07	5.6	4.5	2.1	-	0.216	554	-4.2	1/pm		
7	a	2.76	6.0	5.25	2.0	-	0.216	554	-4.2	1/pm		
8	a	3.10	6.75	4.25	2.0	-	0.216	554	-4.2	1/pm		
9	a	3.45	9.0	4.5	3.5	-	0.216	554	-4.2	1/pm		
10	a	3.45	(perf)	4.0	3.5	-	0.216	554	-4.2	1/pm		
11	a	2.07	3.0	3.0	3.0	-	0.254	540	-0.6	2/1400	Bounce = 23 mm.	
12	a	2.76	6.0	5.5	3.25	-	0.254	540	-0.6	2/1400	Al nose pulled out.	
13	a	3.45	6.5	4.0	2.75	-	0.254	540	-0.6	2/1426	Bounce, projectile angle=87°.	
14	a	3.96	(perf)	3.0	3.5	-	0.254	540	-1	2/1500		
15	a	2.76	9.5	5.0	3.0	-3.5	0.254	540	60.0	-9.9	3/0850	
16	a	2.76	(part)	4.5	2.75	-3.3	0.254	540	57.2	-9.6	3/0908	
17	b	2.07	4.5	4.5	2.75	-2.9	0.254	553	47.4	-4.4	3/1105	Larger debris, bounce = 10 mm.
18	b	2.76	(perf)	4.5	1.0	-2.4	0.254	553	53.0	-4	3/1125	Blue, unexpected perforation.
19	c	1.72	1.25	3.0	1.25	-2.8	0.254	458	58.1	-3.2	3/1331	Bounced out.
20	c	2.24	2.5	3.5	2.5	-2.9	0.254	458	-	-4	3/1344	Tipped slightly, bounce=31 mm.
21	c	2.93	3.25	4.0	3.5	-2.8	0.254	458	-	-4	3/1355	Riverized ice, bounce=18 mm.
22	bl	1.31	2.75	3.5	1.5	-2.8	0.254	349	-	-3.2	3/1405	Blue-smooth bottom in crater.
23	c	3.96	(perf)	4.0	4.0	-2.4	0.254	458	71.3	-	3/1430	
26	a	2.79	8.5	8.0	0.1	-5.5	0.267	540	60.0	-21.5	4/0739	Ice remained in crater.
27	a	2.79	8.25	4.0	3.75	-5.5	0.267	540	56.4	-21	4/0826	
28	a	2.79	9.0	9.5	3.0	-7.5	0.267	540	-	-15	4/0900	60° angle to horizontal.
29	b	3.31	7.5	5.75	3.0	-7.5	0.267	553	-	-9	4/0930	60° angle to horizontal.
31	a	0.86	1.8	1.75	0.5	-4.9	0.267	540	32.2	-1	4/1330	
32	a	1.45	4.6	4.0	2.25	-5.0	0.267	540	36.7	0	4/1340	
33	a	1.90	4.75	4.25	2.25	-5.0	0.267	540	-	0	4/1350	
34	a	2.76	5.1	4.0	2.5	-4.9	0.267	540	59.1	0.8	4/1356	Bounce.
35	a	3.10	4.25	4.0	2.5	-5.0	0.267	540	-	0	4/1410	Bounce.
36	a	3.52	7.5	4.5	3.0	-4.5	0.267	540	-	0	4/1421	
37	bh	3.28	7.4	3.5	2.0	-4.5	0.267	871	-	0	4/1500	
38	a/f	2.76	7.25	3.5	2.0	-4.5	0.279	540	-	0	4/1520	Floater 0.6 m square broke in half upon removal.
39	c/f	2.41	2.1	3.5	2.1	-4.9	0.279	458	-	0	4/1530	Floater 0.6 m square.
40	b/f	2.83	4.25	3.5	1.0	-5.0	0.279	553	-	0	4/1540	Floater 0.6 m square.
41	a/f	2.76	7.75	4.5	2.5	-4.1	0.279	540	-	0	4/1550	Floater 1 m square, 1 small surface crack.
42	a/f	2.76	7.0	5.25	1.25	-6.6	0.279	540	54.4	-10.3	5/1100	Lab ice 0.76 m diam. -5° tilt.
43	a	2.76	6.4	5.5	2.5	-5.6	0.279	540	50.6	-10	5/1145	Deep surface cracks.
44	a/f	2.76	7.5	6.0	2.0	-4.9	0.279	540	-	-9	5/1330	Floater 0.9 m square, surface cracks.

\* 25 mm (1 in.) diameter models; a = cone; b = 0.5 D flat; c = full flat; a/f = floater.

\*\* Measurements normalized to body diameter (1 in.); (perf) indicates complete perforation of the ice sheet.

† Avg temp = temperature over path of penetration.

developed throughout the usual crater region, but the fractured material was not ejected.

We developed a reference test to serve as an index for the test program -- the conical nose shape fired at 55-61 m/s (180-200 ft/s) with a nominal 90° impact angle. We performed this test under the full range of temperatures on all target sizes. We also used this reference test on the

block of laboratory-grown saline ice having a uniform coarse-grained structure to obtain an indication of the effects of structure on depth of penetration.

The following sections present and discuss the findings of this test program in detail.

#### Abrasion during ice entry

To address the question of the nature of the contact between the projectile and ice, we coated the nose of two 0.5 D flat-nose projectiles (shots 18 and 22) with blue layout fluid. Such a coating is thin and brittle and consequently is easily removed by the slightest abrasion. Figure 8 shows the projectile from shot 18 after recovery from the bottom of the test pool. It had completely perforated the sheet and suffered some random scraping during recovery, but gave no evidence of systematic abrasion. Additionally, no bluing was found on the ice at the test point or on the ejecta. Shot 22 penetrated 70 mm (2.8 in.) and also evidenced no abrasion.

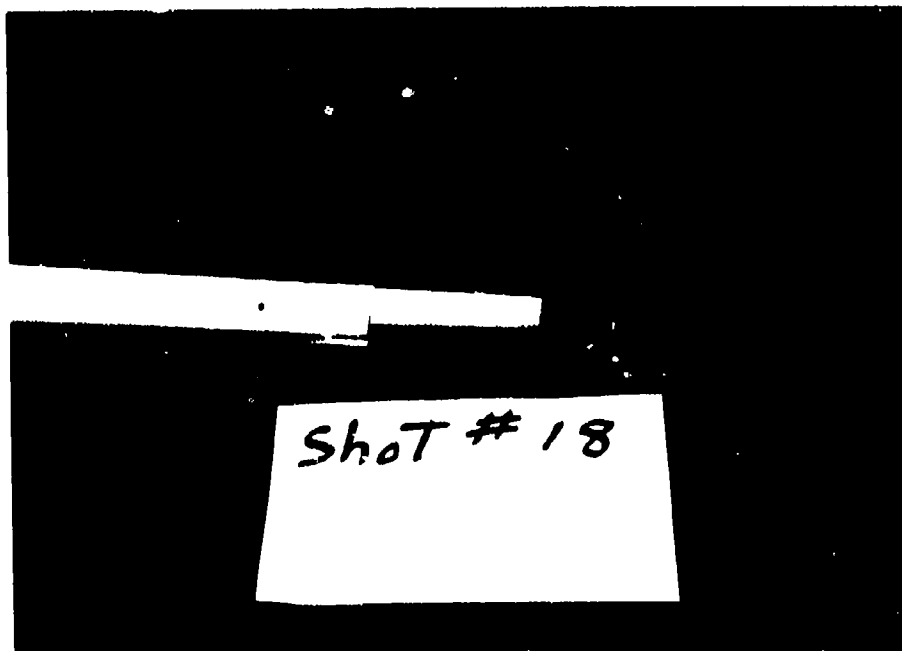


Figure 8. Projectile after shot 18. Note lack of systematic abrasion of the coating of blue layout fluid. This shot perforated the ice sheet.

These observations, along with the extremely smooth appearance of the bottom and walls of the cavity from the penetration shot, lead us to believe that, to some extent, there is pressure melting during penetration that produces a lubricating water film which significantly inhibits abrasion between the ice and the projectile.

#### Macroscopic observations

This section is intended to give the reader an understanding of the appearance of the ice sheets, the crater geometry and patterns of fracture. Figure 9 shows test points after perforation by a flat-nose penetrator (shot 23) and a conical shape penetrator (shot 16). Some debris has been cleared from the cavity in Figure 9a and the water level is evident at the base of the crater. In Figure 9b the fragments have not been cleared.

We removed 17 test points for further examination and thin sectioning. Figure 10 shows a block of ice that had been cut from the sheet. It contained two test points: the projectiles were left in the ice to preserve the geometry of the cavity. At the relatively high ambient temperatures, the cavities would quickly fill with brine that would subsequently freeze when the blocks were brought into the coldroom for examination. Thus, we left the projectiles in place after certain tests to help improve the quality of the analyses that followed the tests.

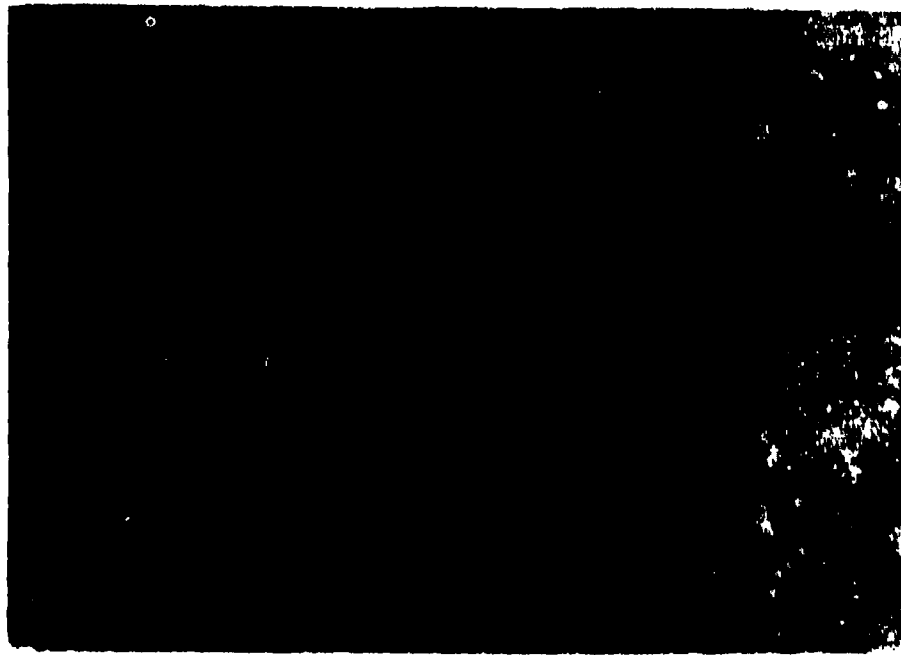
Lower surface temperatures resulted in the behavior seen in Figure 11. For this test, performed before sunrise with an ambient temperature of  $-21.5^{\circ}\text{C}$  ( $-6.7^{\circ}\text{F}$ ), the average ice temperature was between 3 and  $5^{\circ}\text{C}$  lower than in the tests shown in Figure 9. The actual crater is quite small, but there is a large (200-mm-diameter) region of highly fractured material centered on the test point. The lower temperature resulted in increased brittleness near the surface of the ice sheet.

Tests made at a  $60^{\circ}$  impact angle produced craters similar to that seen in Figure 12 for shot 29. The cavity is obviously biased, with most ejecta coming from the region ahead of the projectile. Figure 12b gives a closeup photograph of shot 29. Note that in the above figures there is no evidence of macroscopic cracking extending beyond the crater.

In certain low-velocity shots the projectiles did not remain firmly lodged in the ice. The projectile either was not sufficiently supported and leaned to one side (Fig. 13) or did not penetrate much beyond the cavity depth and consequently fell out altogether (Fig. 14).



a. Shot 16, with a full cone.



b. Shot 23, with a full flat nose.

Figure 9. Typical test points after firing.



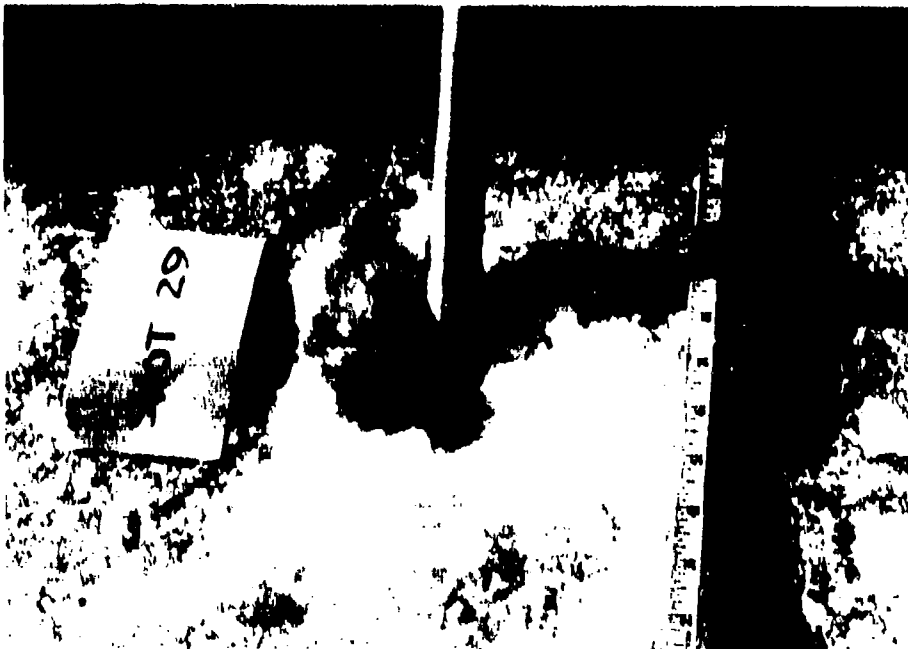
Figure 10. Block of ice containing two test points.



Figure 11. Test point after firing a reference shot at low temperature (air temperature =  $-21.5^{\circ}\text{C}$ , average ice temperature =  $-5.5^{\circ}\text{C}$ ).



a. Shot 29.



b. Closeup of shot 29.

Figure 12. Crater of shot fired at  $60^\circ$  to the horizontal.



Figure 13. Example of a low velocity shot where the projectile did not lodge firmly in the ice, but remained in the cavity (shot 21).



Figure 14. Example of a very low velocity shot that failed to lodge in the ice, noted as a bounce out in Table 2 (shot 32).

## Thin section observations

### General

After testing, the blocks containing the test points were wrapped and stored in a coldroom until sectioning.

We took vertical and horizontal thin sections through and immediately adjacent to the cavity. The objective of these observations was to assess the nature and extent of damage (i.e., crushing and fracturing) to the crystal structure along the path of penetration. This information gives an indication of the mechanics of the penetration process. Material that has been crushed, for example, has a significantly different appearance under cross polarized light than undeformed material. Such observations are easily made in the columnar region of the ice sheet. However, it was often difficult to assess the extent of crushing experienced in the upper 100 mm of the ice because of the irregular granular structure in this region (see Fig. 3).

Another factor that affected the results of the thin section analysis was freezing of water in the cavity after we removed the projectile. Ideally, every penetrator would have remained in the ice until the block containing the test point was removed and thin-sectioned. This was done for only two tests since it was necessary to reuse the other models several times. Also, in a substantial number of the lower-velocity tests, the models failed to lodge in the ice. As a consequence, most of the cavities experienced some degree of flooding and freezing, and the associated thin sections show evidence of this. To make the thin section photographs more meaningful, an outline of the model has been superimposed on certain thin sections to help the reader differentiate between the parent material and the ice that formed after the test.

The following sections address both the penetration tests and the perforation tests that we conducted using the three models discussed above.

### Penetration tests

Figure 15 shows penetration vs gun pressure for all shots that didn't perforate the sheet. As expected, the cone, 0.5 D flat and the full flat-nose shapes experienced decreasing penetration, respectively, at a given gun pressure. The scatter in these data is most probably due to variations in the ice sheet properties as well as to small changes in the projectile's

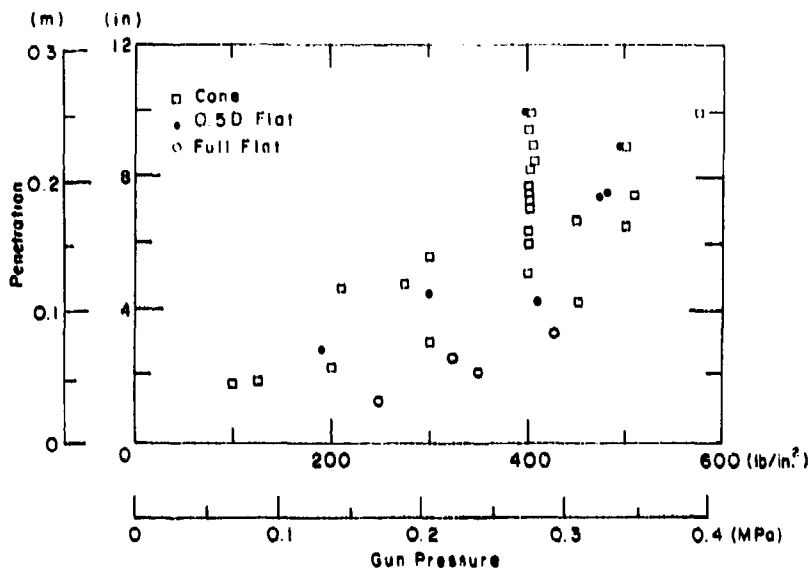


Figure 15. Penetration vs gun pressure for the three nose shapes.

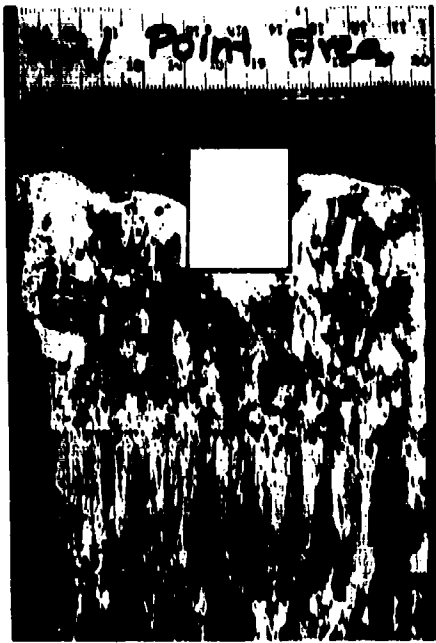
angle of attack and velocity, and measurement errors resulting from the tendency of the models to bounce under certain conditions.

Figure 16 shows thin section photographs of the point area for shots 21 (flat), 22 (0.5 D flat) and 27 (cone). Unfortunately, the freezing problem mentioned above, along with some melting and refreezing that occurs as a result of the thin sectioning procedure, makes the cavity region somewhat ill-defined. The locations of the outlines of the penetrators given in the photographs are based on penetration data and visual inspection.

The thin section from the test using the flat-nose shape (Fig. 16a) shows evidence of a conical region of crushed material extending approximately 0.55 body diameters in front of the penetrator.

The 0.5 D flat-nose model (Fig. 16b) penetrated 70 mm and caused a slight amount of crushing up to approximately 0.43 body diameters ahead of the flat. The material shows some evidence of crushing to a distance of 0.24 body diameters from the tapered portion of the nose. As is the case with many of these tests, the crushing pattern about the circumference of the model is not radially symmetric.

Figure 16c shows the result of a 210-mm-penetration shot by the full cone shape. The ice experienced virtually no crushing ahead of the tip, but crushing occurs irregularly to a distance of about 0.24 body diameters



a. Full flat nose.



b. 0.5 D flat-nose cone.



c. Full cone nose shapes.

Figure 16. Vertical thin section photographs of the point areas for the three nose shapes. The silhouette for each shape has been superimposed on the photographs. The zone of crushing adjacent to the projectiles appears as very fine-grained material in these photographs.



Figure 17. Vertical thin section adjacent to the path of the projectile in shot 27. Path was to the right side of the photograph.

along the conical region. Some relatively large segments of grains survive in the zone of crushing but are surrounded by highly deformed material, as can be seen in Figure 16c to the upper left of the projectile. Figure 17 shows a vertical thin section of material adjacent to the path of the projectile. It distinctly shows a large tapered region of crushed and fractured material extending 100 mm out from the point of impact and approximately 110 mm into the sheet. The actual crater for this test extended only 50 mm from the point of impact. This particular shot (no.

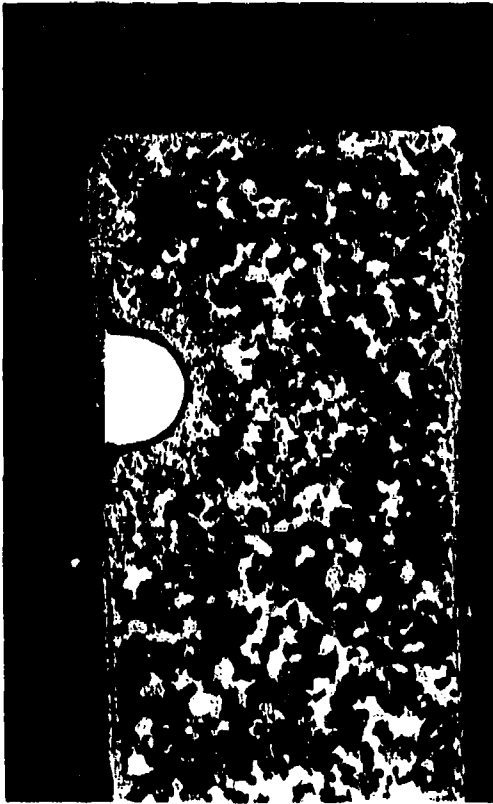


Figure 18. Typical horizontal thin section from the upper part of the ice sheet (shot 15). A silhouette of the projectile has been superimposed on the photograph. Note the fine-grained material adjacent to the projectile that indicates the extent of the zone of crushing.

27) was made at relatively low ambient temperature and, as a consequence, the upper region was significantly colder than in most other tests. Increased brittleness apparently brought about the tendency to develop a large fractured zone in this test, since otherwise identical tests produced craters of similar size but not the extensive fracture zone.

Horizontal thin sections for shot 15 (Fig. 18), which had the same nose shape and gun pressure as shot 27, clearly show the zone of crushed material about the path of the projectile. This zone extends from 0.16 to 0.35 body diameters into the ice. This section was taken approximately 60 mm from the surface of the ice sheet.

Figure 19 gives an indication of the deformation resulting from penetration at an impact angle of  $60^\circ$  to the horizontal. This is a back-lighted section of material that clearly shows the outline of the projectile cavity along with the aluminum tip that came off during penetration and remained imbedded in the ice. The photograph shows the bias in the zones of crushing and fracturing as a result of the  $60^\circ$  impact angle. The deformed material appears shadowed and extends 5 to 10 mm from the cavity



Figure 19. Back-lit thick section of the tip of the cavity from shot 28. The aluminum tip of the nose cone broke off during penetration. The cloudy zones adjacent to the cavity indicate the extent of the crushed material.

along the lower side of the nose section. The crushing is much more extensive on the upper side of the projectile paths, but is difficult to quantify because we do not have appropriate photographs.

There is apparently a transition depth at which the deforming ice moves down and away from the projectile rather than up as during crater formation. Examination of shot 17 (Fig. 20) clearly illustrates this behavior. Total penetration was 4.5 body diameters or 114 mm. Below the bottom of the crater, which is 2.75 body diameters deep, the zone of crushed material is accompanied by several cracks running for 1 to 2 body diameters away from the cavity. The cracks are inclined at approximately  $45^\circ$  to the horizontal.

#### Perforation

A number of shots were fired at sufficient velocity to perforate the ice sheet. With the exception of shot 17, a gun pressure of 3.45 MPa (500 lb/in.<sup>2</sup>) was required to perforate the sheet with any of the three nose shapes. Figure 21 shows vertical thin sections taken along the cavity formed by the conical and full flat-nose shapes with a gun pressure of 3.96



Figure 20. Vertical thin section along the cavity from shot 17. Projectile path was along the left side of the photograph.



a. Full cone nose shape (shot 14).

b. Full flat-nose shape (shot 23).

Figure 21. Vertical thin section along cavities resulting from perforation. Projectile passed to the right in a and to the left in b.



Figure 22. Unusual crater formed by shot 18. Some loose debris has been cleared, but a mound of highly deformed, but intact, material remained around the cavity.

MPa ( $575 \text{ lb/in.}^2$ ). The conical shape in Figure 21a generated a somewhat larger and deeper crater.

Examination of the cavities (right side of photograph in Fig. 21a and left side in Fig. 21b) indicates that the full flat-nosed model left a greater length of smooth, vertical cavity wall than did the conical shape (4.5 vs 3 body diameters starting below the base of the crater). There appears to be no significant difference between the two in the extent of fracturing or crushing in the material adjacent to the cavities. Because of the nature of the experimental setup, we could not make exit velocity determinations for these tests, so it is difficult to make statements regarding the relative efficiency in these two tests.

Shot 18 was anomalous -- a 0.5 D flat-nose projectile launched at a gun pressure of 2.75 MPa ( $400 \text{ lb/in.}^2$ ) perforated the sheet. Figure 22 shows a photograph of the test point area with the loose debris cleared from the crater. Note the mound of intact but highly deformed ice in the crater. No other test displayed this morphology. The cavity wall is very straight to a depth of 200 mm and widens thereafter as seen in Figure 23. It appears that regions along the path of the projectile that were usually



Figure 23. Vertical thin section along the path of penetration of shot 18. Projectile path was to the left of the photograph.

broken free of the ice sheet during perforation were instead crushed in place. These regions are clearly visible along the left side of the thin section photograph in Figure 23.

There is, of course, the possibility that a significant flaw existed in the material, but the local crystal structure is not detectably different from that found at other test points. Additionally, the ice's response to the shot was noticeably different from the norm. The temperature

profile was not significantly different from that of several other shots taken just before and after shot 18 and immediately adjacent to it on the ice sheet.

The cavity formed when a projectile perforates the ice appears to have three distinguishable regions: 1) a crater of approximately 3 to 6 body diameters, 2) a section of relatively constant diameter, equal to the body diameter, and 3) a section of increasing diameter near the exit point. The third section tapers more gradually than the crater but, based on a limited number of observations, appears to have a final diameter approximately equal to the crater diameter.

The crater size does not appear to be greatly influenced by the nose shape but was apparently reduced in diameter at low temperatures since less material was ejected upon impact. Although most of the material about the point of impact was not ejected, a region, roughly the size of a typical crater, was extensively fractured. The length of the constant diameter region of the cavity, and consequently the length of the increasing diameter region, varied according to nose shape.

The photograph of shot 14 (Fig. 21a), with a conical nose, shows a region of relatively constant cavity diameter of between 1 and 2 body diameters in length, whereas the photograph of shot 23 (Fig. 21b), with a flat-nose shape, has a length of approximately three body diameters for this region.

#### Free-floating targets

Several square sections of ice were cut from the main sheet and subjected to the reference shot noted earlier. The targets were all 0.279 m (11 in.) thick and measured 0.6, 0.9 and 1.1 m square respectively (24, 35, and 43 in.). The penetrations were 7.25, 7.50 and 7.75 body diameters, respectively, indicating no significant effect of target size on depth of penetration. However, the radial cracking varied significantly among the three targets.

The largest target (1.1 by 1.1 m) evidenced no macroscopic radial cracks. The 0.9- by 0.9-m target showed surface cracks running from the point of impact to the center of each edge. The smallest target (0.6 by 0.6 m) developed cracks nearly though it, running to the center of each edge. This target broke into four pieces when we attempted to remove it from the water for observation.



Figure 24. Shot 28, fired at an angle of  $60^\circ$  to the horizontal.

#### Additional observations

As mentioned earlier two tests (no. 28 and 29) were conducted to give us an idea of how an angled impact would affect fracturing. Figure 24 shows the impact area for shot 28, which used the full cone nose shape and was fired at  $60^\circ$  to the horizontal. The nose broke off during penetration (see Fig. 19) and the projectile came to rest at an angle of approximately  $45^\circ$  to the horizontal -- the extent to which the nose damage affected the event is uncertain. The length of penetration for shot 28 was within, but to the high side of, the range of the results for the normal-impact shots.

However, the two largest-diameter craters were formed by shots 28 and 29, which were fired at  $60^\circ$  angles to the horizontal. As seen in Figure 24 (shot 28), the crater lies completely to one side of the projectile and the ejecta consist of significantly larger pieces, on average, than the typical normal-impact shots.

Shot 29 (Fig. 12), using the 0.5 D flat cone, came to rest at an angle of  $50^\circ$  to the horizontal. It appears, however, that the projectile's axis initially made a cavity that was at a smaller angle to the horizontal for some distance.

### Crater size and ejecta characteristics

The average surface crater diameter was  $4.4 \pm 1.4$  body diameters and the average depth was  $2.3 \pm 0.9$  body diameters. These dimensions do not appear to vary systematically with nose shape, velocity or temperature. However, the two largest-diameter craters were formed by shots 28 and 29, which, as mentioned earlier, were fired at  $60^\circ$  angles to the horizontal.

From limited observations of the ejecta pattern for penetration shots, the full flat-nose generated ejecta that traveled noticeably higher and that were finer-grained than those created by the other two shapes. The ejecta pattern for the full flat-nose shape became less violent once the ice was perforated.

### Laboratory-grown ice response

As mentioned earlier, we fired a reference shot (full cone nose shape fired at 2.76 MPa [400 lb/in.<sup>2</sup>] gun pressure) into a block of laboratory-grown saline ice having significantly different structural characteristics than the naturally grown sheet. Figure 25 shows a vertical thin section of this material. The average grain size was approximately 5 mm and the salinity averaged 3.5 ‰. Figure 26 shows this specimen after testing. The crater dimensions were within the range of those from the naturally grown sheet but a few radial surface cracks propagated to the edge of the specimen. Recall that there were no radial surface cracks in tests done on the nominally intact sheet. The specimen was left in its heavy cardboard mold for the shot. Interestingly, the penetration of 7 body diameters in the laboratory grown ice was nearly equal to the average of  $7.3 \pm 1.3$  diameters for all the reference shots. This indicates that the significantly larger grain size, the more uniform structure and the lower salinity of the laboratory-grown ice do not have a significant effect on penetration.

### Projectile mass

We conducted two exploratory tests in which projectile mass was varied. We fired two modified 0.5 D flat cone projectiles, shots 22 and 37, that had weights of 349 and 871 g respectively. There are not enough tests to evaluate the effect of projectile mass on the penetration event. However, it is interesting to note that shot 37, using the heavier projec-



Figure 25. Vertical thin section of laboratory-grown saline ice.



Figure 26. Shot 42, fired into laboratory-grown saline ice.

tile fired at 3.28 MPa (475 lb/in.<sup>2</sup>) penetrated to very nearly the same depth as shot 29 using the standard weight projectile fired at 3.31 MPa (480 lb/in.<sup>2</sup>) at an angle of 60°.

#### ADDITIONAL DISCUSSION AND RECOMMENDATIONS

The test site and methodology proved very satisfactory in that we were able to conduct a reasonable number of tests under meaningful conditions. The thin section analysis of the tested material gave useful insight into the mechanics and mechanisms of the penetration event by showing the location and extent of zones of crushing and fracturing for projectiles of three different nose shapes. The test also provided a means to evaluate the relative penetration efficiency of the nose shapes.

There were advantages and disadvantages associated with testing in the field insofar as temperature control is concerned. On the plus side, the temperature gradient is realistic and, provided that the weather through midday is not extremely variable, a relatively large number of tests can be performed under nominally constant thermal conditions. In addition, early morning tests can, at times, provide data at significantly lower surface temperatures. On the minus side, however, are the typical winter weather

patterns that can cause significant thermal fluctuations throughout the day, as well as from day to day, making it difficult to carry out a series of tests under nominally constant conditions.

Testing a floating ice sheet poses the problem that the cavity resulting from a perforation shot immediately fills with water. As a consequence, water quickly freezes in the newly formed voids, significantly changing the appearance of the material to the unaided eye. The appearance of the material formed in this manner can usually be distinguished from the parent material by the examination of thin sections under cross-polarized light. However, this type of examination is more costly than usual photographic techniques. It would be useful to explore alternative techniques for testing the ice on a dry, elastic foundation that would avoid these problems.

In fact, a test series using ice blocks both in and out of the water would allow investigation of the effects of brine drainage on the ice's response to projectile penetration. This type of information is of concern to those who are testing saline ice that has been removed from its growth position for some time before testing. In this circumstance, brine of relatively high salinity drains from the ice, under the force of gravity, by means of interconnected channels, leaving gas-filled rather than liquid-filled voids in the structure. The extent to which this affects the ice behavior during penetration is not well understood but is certainly worth investigating.

The present work serves both to demonstrate the usefulness of a certain test methodology and to show the type of information that can be gained from careful structural analysis of the ice after the test. Being able to see the structural damage via thin section photographs enhances our understanding of the phenomenon. The irregular structural characteristics of the naturally grown ice sheet made it difficult to interpret the thin section photographs but, on the whole, the damage to the material caused by the penetration event was discernable.

The rather unusual crystalline structure of the ice sheet used in this study presented some difficulties. Although limited test results indicate that crystalline structure itself may not be of primary importance to the penetration event, the structural characteristics of the test material should not be ignored. Indeed, some additional testing under a range of

conditions to clarify the role of structure would be helpful. Although the present test results are self consistent, it would be virtually impossible to fully duplicate the test conditions owing to the difficulties in reproducing the structure of the original ice sheet. It is possible to exercise a greater amount of control over the structure of such an ice sheet by seeding the test pool at an appropriate time. This, coupled with reasonable growth conditions, will result in a much more uniform structure than that of the sheet tested in this work. Regarding instrumentation, although it would be a difficult task, an underwater high-speed camera would provide additional useful information on the manner in which the projectile breaks through the sheet.

## CONCLUSIONS

We draw the following conclusions from the work presented in this paper.

1. Standard thin sectioning techniques clearly showed the location and extent of zones of crushing and fracturing in the ice.

2. Projectiles of the stated geometry fired into a naturally grown and nominally intact ice sheet generated no macroscopic cracks other than those directly related to crater formation.

3. Zones of crushing and fracturing were unevenly distributed about the projectile's path but were generally confined to 1 or 2 body diameters from the cavity wall.

4. Length of penetration was a function of nose shape and velocity. There was little difference between the full cone and the 0.5 D flat cone, but the full flat nose was significantly less efficient than the other two.

5. The extent of penetration was not a systematic function of the average temperature over the length of penetration for the range of  $-2.4$  to  $-7.5^{\circ}\text{C}$  ( $27.7$  to  $18.5^{\circ}\text{F}$ ).

6. The projectiles did not experience significant abrasion during penetration or perforation of the ice sheet, as indicated by the lack of damage to a surface coating of blue layout fluid on the projectile nose.

7. For the stated ice thickness, the depth of penetration appeared to be independent of target size for ice ranging from an effectively infinite sheet to rectangular blocks measuring 24 body diameters on a side.

Through-thickness radial cracks appeared in the smallest blocks, while only surface cracks appeared in somewhat larger blocks.

8. The 0.5 D flat cone and the full flat-nose shapes showed varying amounts of crushing ahead and to the sides of the nose, whereas the full cone developed zones of crushing only to the sides of the nose.

9. The length of penetration into a block of laboratory-grown saline ice, having a uniform structure of significantly larger grain size and lower salinity, was the same as in the naturally grown ice sheet, within the range of experimental scatter.